Golgi Structure in Three Dimensions: Functional Insights from the Normal Rat Kidney Cell

Mark S. Ladinsky,* David N. Mastronarde,* J. Richard McIntosh,* Kathryn E. Howell,§ and L. Andrew Staehelin‡

*Laboratory for Three-Dimensional Fine Structure and ‡Department of Molecular, Cellular, and Developmental Biology, University of Colorado, Boulder, Colorado 80309-0347; and §Department of Cellular and Structural Biology University of Colorado School of Medicine, Denver, Colorado 80262-1111

Abstract. Three-dimensional reconstructions of portions of the Golgi complex from cryofixed, freeze-substituted normal rat kidney cells have been made by dual-axis, high-voltage EM tomography at ~7-nm resolution. The reconstruction shown here (~$1 \times 1 \times 4$ μm^3) contains two stacks of seven cisternae separated by a noncompact region across which bridges connect some cisternae at equivalent levels, but none at nonequivalent levels. The rest of the noncompact region is filled with both vesicles and polymorphic membranous elements. All cisternae are fenestrated and display coated buds. They all have about the same surface area, but they differ in volume by as much as 50%. The transmost cisterna produces exclusively clathrin-coated buds, whereas the others display only nonclathrin coated buds. This finding challenges traditional views of where sorting occurs within the Golgi complex. Tubules with budding profiles extend from the margins of both cis and trans cisternae. They pass beyond neighboring cisternae, suggesting that these tubules contribute to traffic to and/or from the Golgi. Vesicle-filled "wells" open to both the cis and lateral sides of the stacks. The stacks of cisternae are positioned between two types of ER, cis and trans. The cis ER lies adjacent to the ER-Golgi intermediate compartment, which consists of discrete polymorphic membranous elements layered in front of the cis-most Golgi cisterna. The extensive trans ER forms close contacts with the two trans-most cisternae; this apposition may permit direct transfer of lipids between ER and Golgi membranes. Within 0.2 μm of the cisternae studied, there are 394 vesicles (8 clathrin coated, 190 nonclathrin coated, and 196 noncoated), indicating considerable vesicular traffic in this Golgi region. Our data place structural constraints on models of trafficking to, through, and from the Golgi complex.

Key words: Golgi • membrane traffic • cryofixation • electron microscopy • tomography

THE Golgi complex is the organelle in which newly synthesized lipids and proteins are modified and targeted for distribution to various cellular and extracellular destinations (reviewed by Farquhar and Palade, 1981). Although the Golgi has been studied extensively for over 100 yr, the relationships between its complex structure and its multiple cellular functions have not yet been elucidated. Current models for the mechanisms by which molecules move through the Golgi are based on data from microscopy, including cytochemical and immunolabeling studies, and from cell free assays of molecular transport events (reviewed by Mellman and Simons, 1992; Orci et al., 1989, 1997). The prevalence of vesicles in the vicinity of the Golgi and the identification of machinery for vesicle formation and fusion have supported the view that vesicles comprise the major mode of transport to, through, and from the Golgi complex (reviewed by Palade, 1975; Rothman, 1994; Schekman and Orci, 1996).

Despite extensive data for the roles of vesicles, there are also data suggesting that tubules may be important for Golgi transport. Electron microscopy has shown extensive tubular networks on the trans face of the Golgi and to a lesser extent on the cis face as well (Rambourg et al., 1979; Roth et al., 1985; Griffiths et al., 1989; Ladinsky et al., 1994). A role for tubules in transport at all levels of the Golgi has also been suggested, based on images of isolated Golgi stacks (Cluett et al., 1993; Weidman et al., 1993). In a different approach, images of living cells have revealed tubules dynamically forming and receding from the trans (Cooper et al., 1990) and cis (Kreis, 1990) faces

Address correspondence to J. Richard McIntosh, Laboratory for Three-Dimensional Fine Structure, University of Colorado, Boulder, Colorado 80309-0347. Tel.: (303) 492-8533. Fax: (303) 492-7744. E-mail: richard.mcintosh@colorado.edu

of the Golgi. Golgi-associated tubules have also been seen using green fluorescent protein to tag transmembrane proteins resident in cis-, medial-, and trans-cisternae (Cole et al., 1996) or the transit protein, VSV-G (Presley et al., 1997; Scales et al., 1997). The relative importance of vesicular vs. tubular Golgi traffic has, however, been difficult to evaluate.

In addition, an older model of membrane traffic, cisternal maturation, is now being reconsidered (Bannykh and Balch, 1997; Mironov et al., 1997; Morré and Keenan, 1997; Glick and Malhotra, 1998). This model suggests that a cisterna is added to the cis face of the Golgi and moves through the Golgi stack, where it is progressively modified by the recycling of Golgi-resident enzymes. The driving force for the progressive movement is thought to be the sequential addition of new cisternae at the cis face. The transport of algal scales provides the best data for cisternal maturation (reviewed by Becker et al., 1995); further evidence comes from the localization of casein in mammary epithelial cells, of collagen in fibroblasts, and of albumin in hepatocytes (Clermont et al., 1993; Dahan et al., 1994; Mironov et al., 1998; Bonfanti et al. 1998). In each case, the molecule to be secreted was found in all Golgi cisternae, but was absent from the transport vesicles on the periphery of the stacks, suggesting that the cisternae themselves, rather than tubules and vesicles, carry secretory proteins through the Golgi. Contrary evidence has been obtained from studies of pancreatic beta cells in which insulin was found in small transport vesicles, as well as in Golgi cisternae at all levels of the stack (Orci et al., 1997).

Paramount to evaluating the evidence put forward for these different views of Golgi transport is a consideration of the strengths and limitations of the methods by which the supporting data were obtained. Biochemical methods start with cell homogenization, which to some extent destroys the complex structure of the Golgi ribbon and leads to the loss of some membrane-associated proteins. Light microscopy of living cells reveals dynamic morphological events, but the method is intrinsically limited to a resolution of ~200 nm, so interactions between and among Golgi cisternae, which are separated by ~20 nm or less, are invisible. Furthermore, it is impossible to distinguish membranous tubules from linear rows of vesicles in the light microscope.

EM provides the resolution necessary to make these discriminations, but there are two formidable problems associated with this methodology. First, chemical fixation takes seconds to minutes to immobilize cellular processes, and different cellular components are fixed at different rates (reviewed by Gilkey and Staehelin, 1986). When one hopes to characterize a highly dynamic structure like the Golgi, this limitation is severe. Second, most imaging technologies for EM, including those that involve rapidly frozen or other well-fixed materials, draw conclusions from very small, essentially 2-dimensional (2-D),[1] samples. The Golgi ribbon and related structures (e.g., tubules, vesicles, and exit sites from the endoplasmic reticulum) cover an extensive region of the cytoplasm. EM of thin sections selected from multiple cells and/or multiple regions from a single cell, even freeze-fracture replicas of isolated fractions, cannot reveal the complete 3-D organization of the Golgi and the structures involved in traffic to, from, and through it.

To solve these problems, we require high resolution 3-D structural data that describe large volumes of Golgi preserved by optimal methods. Failure to meet all of these requirements has limited the conclusions that could be drawn from previous work; e.g., where chemically fixed and specifically stained Golgi regions were analyzed by EM tomography of individual 250-nm sections (Ladinsky et al., 1994). The data in Ladinsky et al. (1994) provided clear evidence that tubules extend from multiple trans cisternae, reaching into the region trans from the Golgi stack. Budding profiles with distinct coat structures formed from these tubules, and single tubules produced buds with only one coat type. It was not possible, however, to determine if an individual cisterna could produce vesicles with more than one coat type without sampling a larger volume of the Golgi ribbon. A major goal of the current study was to address this question by using more advanced methods for sample preparation and larger volumes for 3-D image analysis.

To this end, we have united two modern structural methods to provide a reliable view of a significant portion of the Golgi ribbon in a normal rat kidney (NRK) cell: fixation by ultra-rapid freezing, followed by freeze substitution to prepare specimens for EM analysis, and dual-axis, high-voltage electron microscope (HVEM) tomography of serial, semi-thick sections to provide high resolution images in 3-D. Ultra-rapid freezing is widely accepted as a method that is superior to chemical fixation, due to its ability to immobilize all molecules in a cell within milliseconds (reviewed by Gilkey and Staehelin, 1986). Samples that have been rapidly frozen and subsequently freeze substituted at −90°C are also more likely to retain the features of even the most labile cellular structures. Dual-axis tomography, based on HVEM of comparatively thick sections, provides 3-D images at ~7 nm resolution (Penczek et al., 1995; Mastronarde, 1997). This constitutes an improvement of 15–20-fold over the 3-D resolution available from conventional, serial sections for EM (Sesso et al., 1994). It is also a significant improvement relative to the HVEM stereo imaging of thick sections of chemically fixed cells that has been used effectively to study Golgi architecture (reviewed by Rambourg and Clermont, 1997).

The results of this study provide a new view of Golgi structure in cultured mammalian cells with a constitutive secretory pathway. Even though only fractions of a cell's entire Golgi ribbon have been reconstructed, several novel features of Golgi structure have been revealed and other features, demonstrated in earlier work, have been confirmed. This study provides both objective and quantitative information about 3-D organization, and we suggest that these data present a significantly improved baseline of information with which to evaluate current hypotheses about the functional organization and dynamic behavior of the Golgi complex. They also provide new frameworks within which to plan future work.

1. *Abbreviations used in this paper:* 2-D, 2-dimensional; CGN, cis-Golgi network; ERGIC, ER-Golgi intermediate compartment; HVEM, high-voltage electron microscopy; NCR, noncompact region; NRK, normal rat kidney; VTC, vesicular tubular cluster.

Materials and Methods

Cell Culture

Normal rat kidney cells were cultured at 37°C in DMEM (Sigma Chemical Co.) supplemented with 8% fetal calf serum. For specimen preparation, cells were grown to ~80% confluency on Formvar-coated, carbon-stabilized, glow-discharged 100-mesh gold EM grids.

Plunge Freezing and Freeze Substitution

Cells were maintained at 37°C until within 15 s of the freezing step. Grids with cells attached were picked up with self-closing forceps and rinsed briefly (~10 s) in DMEM containing 3% 70-kD Ficoll (Sigma Chemical Co.), which serves as an extracellular cryoprotectant. The addition of Ficoll, including its contaminating salt, increased the osmolarity of the medium by <3%. The forceps were then attached to the piston of a plunge-freezing apparatus. All excess fluid was carefully removed from the grid with filter paper (#1; Whatman Inc.), and the piston was released to plunge the grid rapidly into a pool of liquid ethane chilled to −174°C by a surrounding bath of liquid nitrogen. The rate at which samples are cooled by this method is ~104°C/s (Gilkey and Staehelin, 1986). After plunging, grids were quickly transferred to liquid nitrogen and prepared for freeze substitution.

For freeze substitution, the samples were transferred first to cryostorage tubes (Nalge-Nunc International) containing 1% glutaraldehyde and 0.1% tannic acid in acetone and maintained at −90°C for 2 d. They were then allowed to warm slowly to −50°C over the course of ~6 h, at which point the substitution solution was replaced with a precooled (−50°C) solution of 2% OsO_4 and 0.01% uranyl acetate in acetone. Samples were then allowed to warm from −50° to 4°C over 24 h. The samples were rinsed three times in acetone, infiltrated with increasing concentrations of Epon-Araldite resin, and flat-embedded between two Teflon-coated glass microscope slides (Miller-Stephenson). The resin was polymerized at 60°C for 2 d.

Sample Preparation and Selection

Embedded samples were observed by phase-contrast light microscopy and areas of apparently well-preserved cells were excised from the plastic "wafer" and remounted with epoxy glue onto plastic stubs in an orientation suitable for cross-sectioning. Thin (30–40-nm) sections were cut on a UltraCut-UCT ultramicrotome (Leica Inc.), transferred to Formvar-coated copper-rhodium slot grids, stained with 2% aqueous uranyl acetate and Reynold's lead citrate, and observed on a JEM-100CX transmission EM (JEOL U.S.A. Inc.) to determine specimen quality and to select suitable samples.

Blocks that yielded cells with distinct regions of well-preserved Golgi were returned to the microtome where ribbons of 6–12 serial 250-nm sections were cut and transferred to slot grids. Sections were stained for 15 min with 3% uranyl acetate in 70% MeOH, and then 3 min with Reynold's lead citrate. After staining, 10 nm colloidal gold particles were added to both sides of the grid to serve as fiducial markers for aligning the series of tilted images. A second layer of Formvar was cast onto the section side of the grid, and both sides of the grid were carbon coated to enhance stability.

High Voltage Electron Microscopy and Dual-Axis Tilt-Series Imaging

Procedures for image acquisition and dual-axis tomography were as described previously (Mastronarde, 1997). In short, grids were placed in a stage capable of both high tilt and specimen rotation in the plane of the grid. They were observed in a JEM-1000 HVEM (JEOL U.S.A. Inc.) operating at 1 MeV. Once a suitable Golgi region was selected, the sample was tilted from +60° to −60° at 1.5° intervals, and 80 images at 15,000× were collected on film (23D56; Agfa-Gevaert N.V.). The grid was then rotated by 90°, and a similar series was taken. An area corresponding to 3.84 × 1.86 μm was digitized at a pixel size of 2.35 nm. Images were aligned and a tomogram was computed from each tilt series. To merge the two single-axis tomograms into one, they were registered to each other with a warping procedure, rather than a single linear transformation (Mastronarde, 1997), because nonlinear distortions between the two tomograms were evident over such a large volume. The above procedure was followed for each of the four serial sections.

It is difficult to specify the resolution of our reconstruction with certainty. Standard formulas (Radermacher, 1992) give a resolution of 7.8 nm for each of our single-axis tomograms in the x direction (perpendicular to the tilt axis). For several reasons (e.g., the appearance of the unit membrane bilayer in some areas), we estimate that the resolution in the x–y plane for our dual-axis tomograms is ~6 nm. Because of the limited range of tilt angles, resolution is 1.3× worse in the z direction (Mastronarde, 1997), or ~8 nm.

The tomograms from adjacent 250-nm sections were aligned with each other by examining 2.4-nm slices extracted from the tomograms parallel to the plane of each section; the bottom-most slice from the first section was aligned to the top-most slice from the next. This method was similar to that of Soto et al. (1994), except that we aligned the pair of slices with a general linear transformation, which incorporates an overall size change and stretch along one axis. Such a transformation was necessary to obtain a good match across the section boundaries, which in turn was important for being able to track features across a section boundary. The parameters of the transformation were adjusted manually to give the best apparent fit, as judged by viewing the two slices in rapid alternation (Kremer et al., 1996). The linear transformation gave an excellent alignment of the slices across two of the boundaries and an adequate match across the third, with displacements of two to three pixels in some regions of the reconstruction.

The alignment process was complicated by an evident loss of material between sections. The amount of loss was assessed by examining the change in image features across a section boundary; vesicles cut by the sectioning process were particularly useful. Approximately 15–25 nm of material appeared not to be present in the tomogram. On rare occasions, these gaps led to ambiguity in establishing connectivity between vesicular or tubular elements.

Once the alignment parameters were determined, aligned regions (1,632 × 440 × ~65 pixels) were extracted from each of the four sections and stacked into a single volume 257 pixels thick. The model presented here was constructed from this volume. The thickness of stained material within each section of the tomogram was only 150 nm, partly due to the loss of material just described, but mostly due to the collapse in section thickness that rapidly follows the initial observation of plastic sections (Luther et al., 1988). A 2.4-nm slice from the tomogram parallel to the plane of section thus corresponds to ~4 nm of unthinned material. Before viewing and analysis, the z dimension of our model was stretched by a factor of 1.65 to bring the total z extent of the model to 1.0 μm (four sections of 250-nm each).

Modeling

The tomographic reconstruction was interpreted and modeled using Silicon Graphics computers running the IMOD software (Kremer et al., 1996). Each compartment in the reconstructed Golgi region was considered a distinct "object," and a different color was assigned to each object. The portion of each object that was visible in one tomographic slice was traced as a "contour" overlaid on the image. Objects were modeled one at a time. Before modeling an object, the operator studied it throughout its entire volume to make an initial assessment of its connectivity. Modeling began at a slice within the data set where the object was most distinct; it was then traced through adjacent slices in both directions to assure that all compartments associated with that object were included in the model. This often involved backtracking to include compartments that in some slices were separated from the main body of the object, but in others were obviously attached to it. If a coat was present on a budding profile, its position was indicated by stippling.

The resolution of the tomogram allowed for most objects to be followed and modeled with complete confidence. However, some tubules in the noncompact region, budding profiles, and the regions at the boundaries of physical sections, posed a challenge. These regions were given particular attention by using the "slicer" tool in IMOD that allows the operator to view image data from any angle.

Free vesicles were modeled in one of two ways. Vesicles located within openings in the Golgi stack were modeled as described above. Their small radius, combined with the slightly reduced resolution of our tomograms along the beam axis, led to a modeling artifact. Each of these vesicles appears slightly extended parallel to the beam axis. Free vesicles located around the periphery of the stack were modeled by placing a simple sphere at that location. Vesicles with different coat structures were marked by spheres of differing size and color.

After its completion, the model was smoothed by fitting local polynomials to the surfaces and replacing each point with a corresponding point

from the fitted surface. This smoothing compensated, in part, for the difficulty in drawing contours that shifted smoothly in position from one plane to the next. A mesh of triangles was then computed to define the surface of each object (Kremer et al., 1996), so that objects could be viewed with standard lighting techniques. Surface areas in the model were computed from the triangular meshes, and internal volumes were determined from the contour information, after adjusting for the thickness of the membrane inside the contour. The sizes of openings in the cisternae were measured with a program devised for this purpose. The operator first marked the top and bottom of each opening with model points. The program then found the projected area of the opening from the angle of view that gave the greatest area. For each opening, the diameter of a circle with the same area was computed and used for analysis.

Results

Technical Advances Enable the Imaging of Organelles with Unprecedented Three-Dimensional Reliability

Accurate 3-D modeling of cellular fine structure requires both excellent preservation of the biological sample and a method for precisely tracking objects in space. Here we have used a combination of cryofixation and dual-axis, HVEM tomography to model the Golgi complex with a 3-D resolution of ~7 nm. The quality of the structural preservation provided by fast freezing and freeze substitution, as well as the resolution of the tomographic "slices" used in this study, are demonstrated in Fig. 1 a. The Golgi cisternae of this cultured NRK cell are smooth and comparatively straight. The spacings between adjacent cisternae are remarkably uniform, and all of the surrounding cytoplasm appears to be well preserved, including cytoskeletal elements such as microtubules (Fig. 1 a, red arrow). The tomographic slices used in this study are only 4-nm thick, so they offer a significant advantage over typical serial "thin sections" (~60 nm) for tracking convoluted membranes in 3-D. This advantage is evidenced by the very slight but detectable change in the microtubule from Fig. 1, a to b, which is the adjacent tomographic slice.

Nearly all the budding profiles on Golgi cisternae displayed a coat of some kind. The fixation and staining procedures employed in this study have enabled us to distinguish membrane bilayers (Fig. 2, a and a′), noncoated vesicles (b, c, and c′), nonclathrin–coated buds and vesicles (d, e, and e′), and clathrin coats (f, f′, g, and g′). Although clathrin and nonclathrin coats can be distinguished from uncoated vesicles, we cannot distinguish COPs from "lacelike" coats (Ladinsky et al., 1994). Our description of coats is therefore limited to clathrin and nonclathrin.

The reconstruction shown here is derived from four serial 250-nm sections that yielded 257 tomographic slices, like the ones shown in Fig. 1, a and b (slices 175 and 176). All of these slices were used to model the shapes and positions of seven Golgi cisternae and the nearby ER, vesicles, and tubules. The boundary of each Golgi element was traced to represent its membrane in each tomographic slice, as described in Materials and Methods. Different colors were used to represent each cisterna and its associated structures (Fig. 1 b). The quality of the individual images and the thinness of the slices made for essentially no ambiguity in the connectivity of the different Golgi compartments. This factor allowed us to look carefully for places where adjacent cisternae might fuse or connect, but we found none.

The volume selected for this reconstruction (~$1 \times 1 \times 4$ μm) included two compact Golgi regions separated by a noncompact region (NCR); together, these constituted ~5% of the cell's entire Golgi complex, based on estimates from low magnification EM (not shown). When the resulting model is displayed in its entirety, it is so complex that single views are not as informative as one would like (Fig. 1, c and d). Although the ER at the top and bottom and the well ordered cisternae of the compact regions are clear, the less ordered regions of the model are more difficult to visualize. The fine details within the model are obscured by all the features that are superimposed. We therefore present our results by disassembling the model in various ways.

Dissecting the Golgi with Computer Graphics

One of the most informative views of the model is shown in Fig. 3 (top), where the individual layers, including the Golgi cisternae C1–C7, are displayed as separate objects, each viewed from its cis-Golgi side. The cis-trans polarity of this Golgi region was deduced from the orientation of the cis-Golgi wells (Rambourg and Clermont, 1997) and the fact that only cisterna C7 displayed buds coated with clathrin. Clathrin has been shown to be associated only with the trans side of the Golgi (reviewed by Farquhar and Hauri, 1997). Other features of the model are highlighted below (see Figs. 4–9).

Structural Characteristics of Compartments Neighboring the Cis Golgi

On the cis side of the reconstructed Golgi is a layer of ER (Figs. 1 c and 3, blue-gray structures). This ER displays typical tubular and cisternal domains but no budding profiles. The lack of budding suggests that the cis ER reconstructed here was not functioning as an "exit site" at the time it was frozen. The paucity of cis ER in this model reflects the limited volume digitized.

Between the cis ER and the stacks of Golgi cisternae, there is a layer of branched tubular structures and flattened sacs (Figs. 1, c and d, and 3, yellow structures). Most of these 44 discrete elements are concentrated over the compact regions of the cis-most cisterna (C1), suggesting a specific association. Based on its position and morphology, we interpret this layer as part of the ER-Golgi intermediate compartment (ERGIC). None of the ERGIC is, however, closely adherent to the surface of C1 (Fig. 1, c and d). Some of the ERGIC elements exhibit structures that resemble budding or fusing vesicles, but none appears coated. There is no continuity between the ERGIC elements and either the cis ER, C1, or any of the other Golgi cisternae. The ERGIC is structurally different from all of the Golgi cisternae, and indeed an examination of the yellow contours in Fig. 1 b suggests that if only 2-D information were available, one might not identify the ERGIC as a compartment with a distinct structural character, but rather as a collection of polymorphic vesicles. The ERGIC region also contains many spherical vesicles, as shown in Fig. 3 (bottom). A single microtubule enters the ERGIC region from the edge of the sample and runs approximately parallel to the plane of the Golgi cisternae (Fig. 1 a, red arrow).

Common Structural Features of the Golgi Cisternae

Each of the compact regions in this Golgi model consists of seven stacked cisternae. There is also a partial cisterna (C6′), which is found only on the right side of the right stack (Figs. 1 c and 3). Bridges across the NCR connect the two parts of three cisternae (C1, C3, and C6), while C7 nearly covers the NCR, blocking most of its access to the trans side of the Golgi. Bridges were not detected between the parts of C2, C4, and C5, but these cisternae may be connected outside the reconstructed volume. There are no lateral, vertical, or branched connections between cisternae at different levels in the stacks.

Although each cisterna is distinct, these structures possess many features in common. All cisternae are interrupted by openings of three different size classes (discussed below). All display buds, which are usually located at their margins or at the edges of holes (Fig. 3). On C2 and C6 budding structures are also found at the distal ends of tubules that extend from the margins of the cisternae.

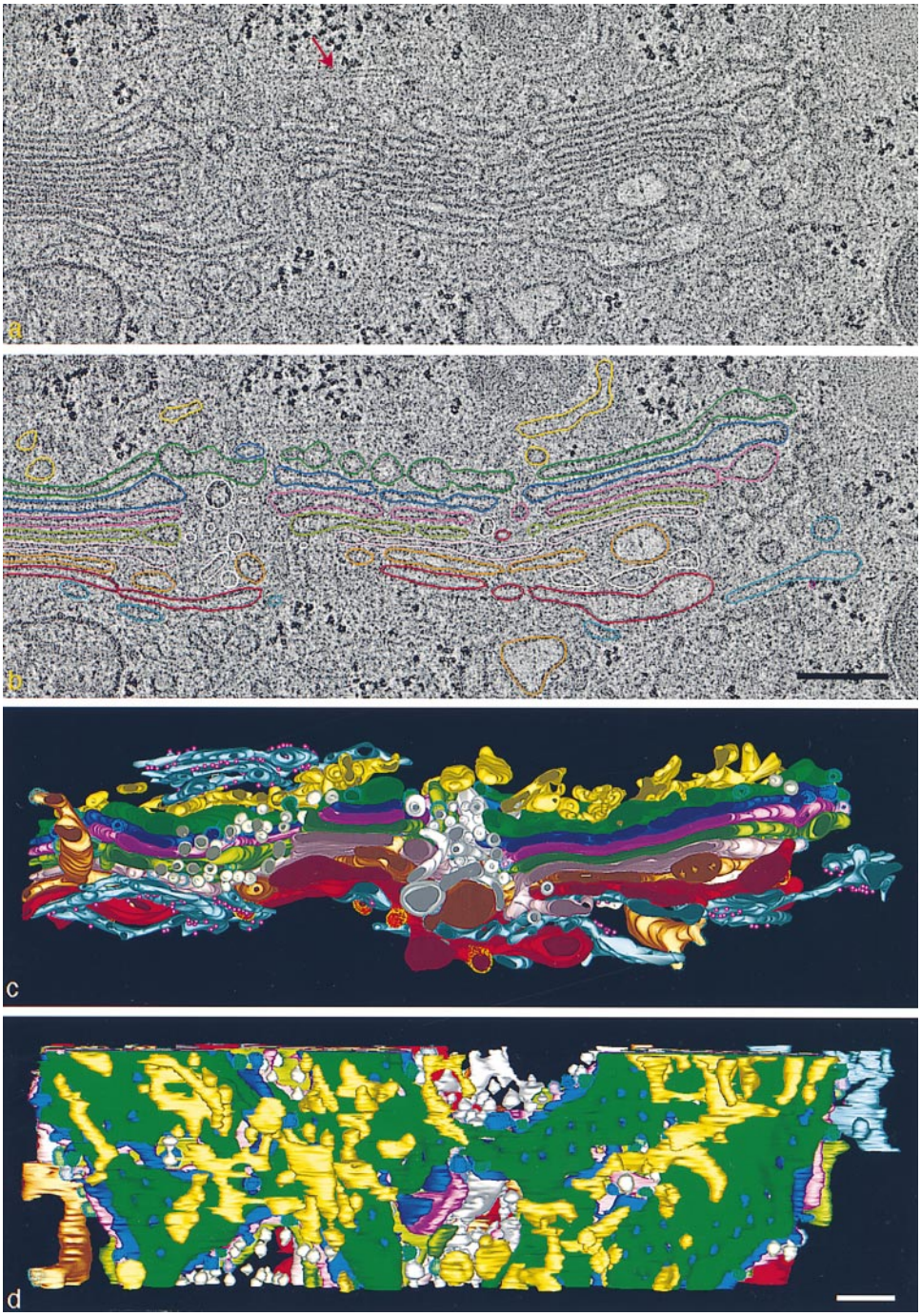

Figure 1. HVEM tomographic reconstruction of a portion of the Golgi ribbon from a fast frozen, freeze-substitution fixed NRK cell. Two serial 4-nm slices extracted from the tomogram are shown in a and b. Comparison of the images shows how little is changed from one such slice to its neighbor; e.g., the position of the microtubule (red arrow). (a) Membranes of individual Golgi and ER cisternae are clearly seen. (b) In analyzing the data, different cisternae were modeled by placing points along the membranes that delimit them, connecting the points with colored line segments, and building closed contours that model the different membrane compartments of a given slice. c and d are renditions of the surfaces fit to all of the contours for each object modeled in this Golgi region. The model viewed in c is in the same orientation as the tomographic slices. d shows a cis-side view with the cis ER removed to provide a better view of the ERGIC elements and the underlying Golgi cisternae. The 44 elements of the ERGIC are discontinuous, display no coated budding profiles, and do not appear to be flattened against the cis-most cisterna. Free vesicles in wells and the NCR (white) have unrestricted access to the cis side of the stack. The colors used to represent different components of the model are the same in all figures: ER, blue-gray; ribosomes, small purple spheres; ERGIC, yellow; Golgi cisterna: C1, green; C2, purple; C3, rose; C4, olive; C5, pink; C6, bronze; C7, red. Polymorphic structures in the NCR are light pink and gold. Non–clathrin-coated budding profiles on cisternae C1–C6, blue stippling. Clathrin-coated buds on C7, yellow stippling. Bars, 250 nm.

C6 and C7 also show one bud each forming from their flattened surfaces (see Figs. 3, C6, lower middle, and 5 e, lower middle, respectively). Most of the buds associated with the Golgi cisternae appear coated. The few that lack coats invariably also lack a necklike constriction, suggesting that they are images of fusing vesicles.

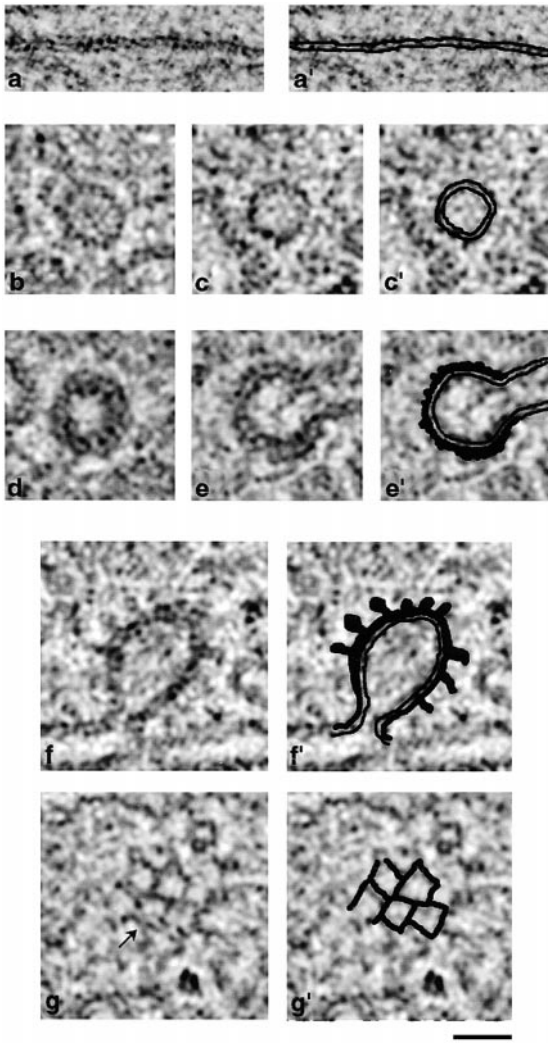

Figure 2. Identification of membranes and coat structures in tomographic images. Due to the thinness of tomographic slices (4 nm) and the limitations of the tomographic technique, membranes appear different from conventional thin sections (40–80 nm). Here we illustrate membranes and coats in composite images, each the sum of three adjacent tomographic slices. Panels on the right include interpretive diagrams. a and a′ show detail of a Golgi cisternal membrane that shows the two leaflets of the lipid bilayer with some clarity. b, c, and c′ show noncoated vesicles; the membrane thickness appears similar to that in a, and the two leaflets of the bilayer are occasionally discernible. d, e, and e′ show a non–clathrin-coated vesicle and bud, respectively; the two leaflets are easily seen, but the darkly stained coat structure is indistinguishable from the outer leaflet. f and f′ show a clathrin-coated bud in cross-section with characteristic spike structures. g and g′ show the cagelike structure on the surface of a clathrin-coated vesicle. The arrow in g indicates a single clathrin triskelion. Bar, 50 nm.

Aligned Cisternal Holes Form Wells

When the cisternae are aligned, their larger holes line up to form "wells." In contrast, the smaller openings, called fenestrae, are not in register from one cisterna to the next. Free vesicles and budding profiles attached to the cisternal edges that delineate the wells fill much of the well volume (Fig. 4 a). Note that the nonspherical appearance of the vesicles is probably due to the stretching artifact described in Materials and Methods. There is also a tapering tubule, depicted with Fig. 3, C5, that extends from the edge of the model into one of the wells (Fig. 4 b). Cis-Golgi wells are those that are open to the cis side of the stack but are closed at the trans side (as defined by Rambourg et al., 1979; Fig. 3). Fig. 3 contains two cis-Golgi wells in the left compact region and one in the right. These wells penetrate through different numbers of cisternae: C1–C3 and C1–C6, respectively. Another set of aligned holes in the right stack has no opening to the cis face; its access to the cytosol is through an opening on the side of the stack (Fig. 3, C2–C6, right edges). It too contains profiles of coated budding vesicles. Yet another set of aligned openings forms a "trans-well," but this well lacks both budding and free vesicles (Fig. 3, C2–C5, lower left side).

Tubular Extensions of Cis and Trans Cisternae Reach Past Adjacent Cisternae into the ERGIC and TGN Regions

Tubules with budding tips project from the margins of both cis- and trans-side cisternae; they extend outwards, roughly perpendicular to the planes of the cisternae (Figs. 1 c and 5, a and c–e). Tubular extensions from multiple trans cisternae have been used as a defining characteristic of the trans-Golgi network (Rambourg et al., 1979; Ladinsky et al., 1994), but tubules emanating from cis cisternae have been reported less frequently (Rambourg and Clermont, 1997). Both of the tubules that emanate from C2 end in the ERGIC region with a coated bud (Fig. 5 a, short arrows). Cisternae C5, C6, and C7 all extend tubules into the region that lies trans from C7 (Fig. 5 c). The C6 cisterna is unique in that it extends one tubule in the cis direction as well as one in the trans (Figs. 1 c and 5 d, arrowhead, and e). The cis-oriented tubule on the left passes all five of the preceding cisternae and finally ends in the ERGIC region with a coated bud.

The Noncompact Region Contains Small Vesicles and Polymorphic Membranous Elements

The 3-D resolution of our model has enabled us to define the contents of an NCR better than has previously been possible. Most workers show this region filled with vesicles that lie between slender bridges connecting cisternae of adjacent stacks (e.g., Rambourg and Clermont, 1990). Fig. 5 b illustrates at higher magnification a projection of the elements in the NCR that are not connected to cisternae. The region contains numerous vesicles, which are colored white, in addition to larger polymorphic elements. Fig. 6 shows most of the elements of the NCR that are attached to cisternae. These three sets of bridges and tubules are complex and, like some of the free elements, polymorphic. The origin of the free polymorphic elements is a fascinating question. Several of them resemble the tubular and

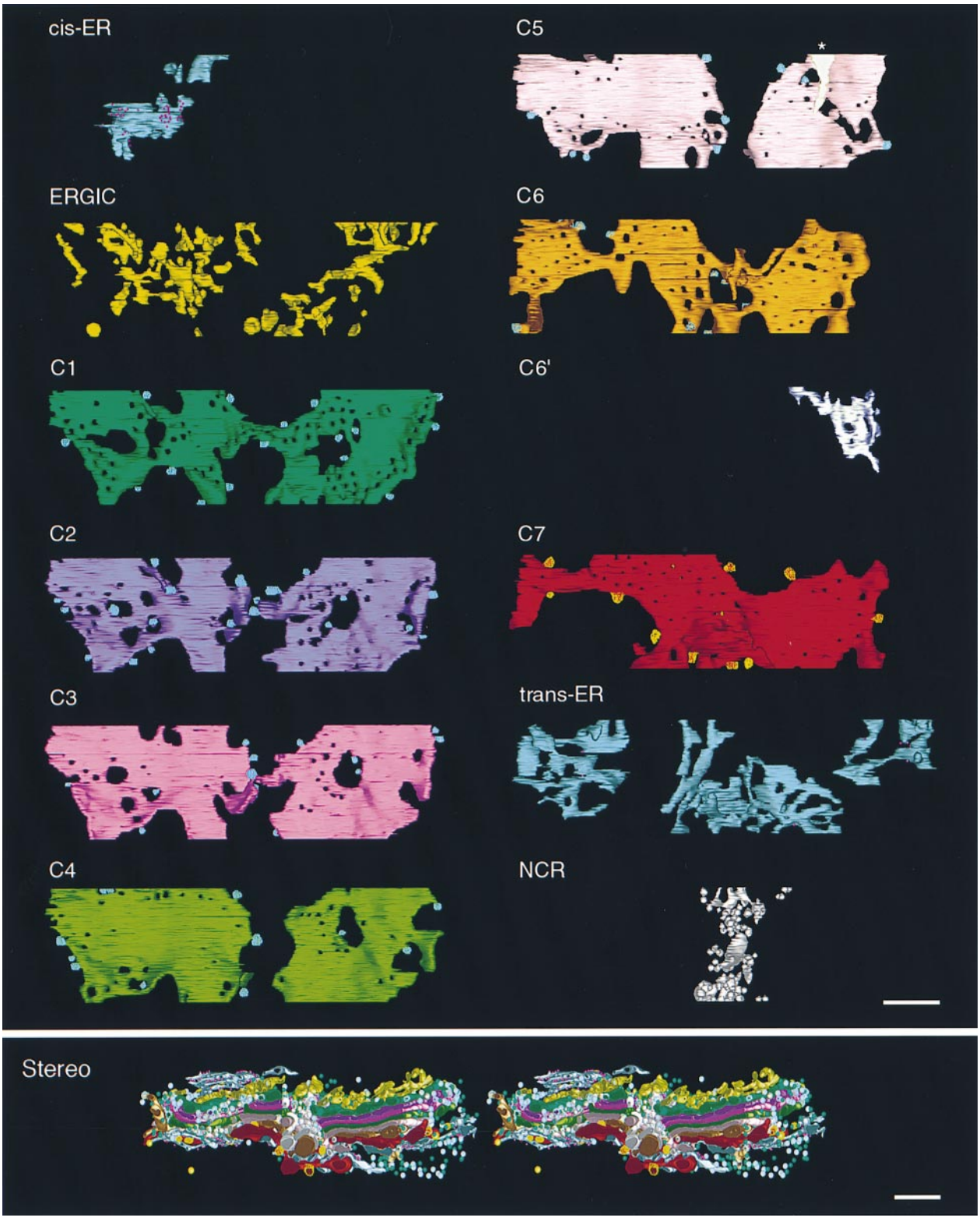

Figure 3. (Top) Successive layers of the Golgi model, each viewed from its cis side. cis-ER, the ER on the cis side; ERGIC, the ERGIC layer; C1–C7, the cisternae in cis-to-trans order; trans-ER, the ER on the trans side. C6′ is a partial cisterna, positioned between C6 and C7, which we interpret as ER. The starred object in C5 represents a membrane tubule of unknown origin. The noncompact region (NCR) displays all the elements lying between the two compact regions but not connected to either. All coated vesicles budding from cisternal margins are highlighted with stippling. The trans-most cisterna, C7, is the only one that is budding clathrin-coated vesicles (yellow stippling). All fenestrae and holes within each cisterna are included. (Bottom) Stereo image of the complete model including the free vesicles that surround the stacks (not shown in Fig. 1). Yellow, blue, and green spheres represent clathrin-coated, non–clathrin-coated, and non-coated vesicles, respectively. Bars, 250 nm.

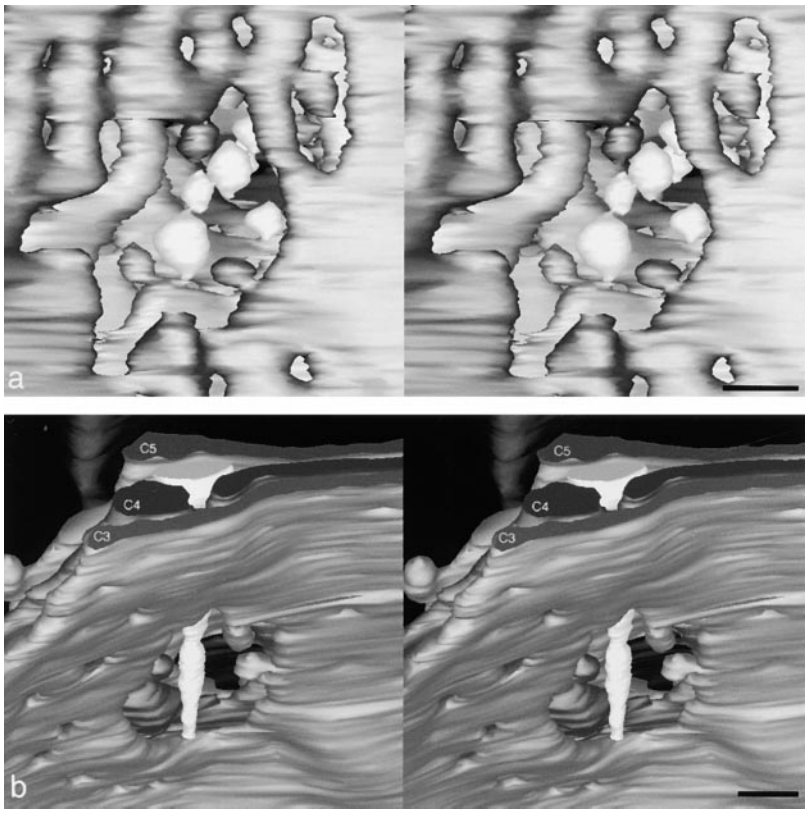

Figure 4. Stereo images of the cis-Golgi well in the right compact region of the model. a shows a view from C1 to C6, revealing the depth of this well and the extent to which it is filled with buds and vesicles. The probable reason why vesicles are not round is discussed in Materials and Methods. b shows the same well as defined by holes in C3–C5, displaying the arrangement of the tapered tubule that enters this model from the side (Fig. 3, C5, star). Bar, 100 nm.

flattened elements of the ERGIC (compare the yellow elements in Figs. 1, c and d, and 5 a with the gold elements in 5 b). Others are more rounded and have a smaller surface-to-volume ratio than any elements of the ERGIC (Fig. 5 b, pink elements). Some disconnected elements of both colors resemble the bridging and tubular structures that are connected to cisternae in the NCR (Fig. 6).

Large Numbers of Free Vesicles Surround the Cisternae

Fig. 6 depicts a total of 394 vesicles, including the free vesicles in the wells, the NCR, and the peripheral regions of the reconstructed Golgi. Of these, only eight are clathrin coated. The remaining population is nearly equally divided between non–clathrin-coated (190) and noncoated vesicles (196). The total surface area of the vesicle membranes is 4.9 μm^2, comparable with the surface area of one cisterna of our model, and their total volume is 0.025 μm^3, similar to the volume of C5 (Fig. 7). A majority of the non–clathrin-coated vesicles is localized around the cis half of the stacks, whereas more of the noncoated vesicles are around the trans half (Fig. 3, bottom). This figure also shows that the distribution of vesicles at the trans side of the model is highly nonuniform.

The Trans ER Forms Intimate Associations with Two Trans-Golgi Cisternae

The trans ER shown in Fig. 5, d and e, flattens and closely abuts the trans faces of both C7 and C6. These appositions appear as tight as those between adjacent Golgi cisternae. In addition, the trans ER is wrapped around parts of C7 (Fig. 5 d, arrow). Ribosomes are associated with the trans ER on only the side that is distal to the Golgi. We have also observed such interactions in both PtK and CHO cells after fast freezing/freeze substitution (data not shown). Our observations suggest that this relationship is characteristic of mammalian Golgi. The trans ER lacks buds, suggesting that there is no vesicular transport between this compartment and the Golgi. The partial cisterna (Fig. 3 C6′) located between C6 and C7 has the same general morphology as the trans ER, except that it is free of ribosomes, it lacks coated buds, and displays an intimate association with both trans-Golgi cisternae.

Generality of These Qualitative Observations

The descriptions presented above are all based on one model of a portion of the Golgi ribbon from one cell. We think, however, that they are more representative of the structure of NRK Golgi than this small sample might suggest. While developing our methods for specimen preparation, we prepared ~40 sets of samples by cryofixation and freeze substitution, and then evaluated them by serial thin sectioning and in some cases by HVEM tomography. All major observations described here (lack of connectivity between nonequivalent cisternae, association of clathrin with only the trans-most cisterna, the existence of tubules projecting from multiple cisternae, and the close association of trans ER with multiple trans-Golgi cisternae) have been reproduced in two or more cells and sometimes in multiple cell types. The labor of detailed modeling (6×10^6 data points recorded here) has precluded equivalent documentation of a large number of cells.

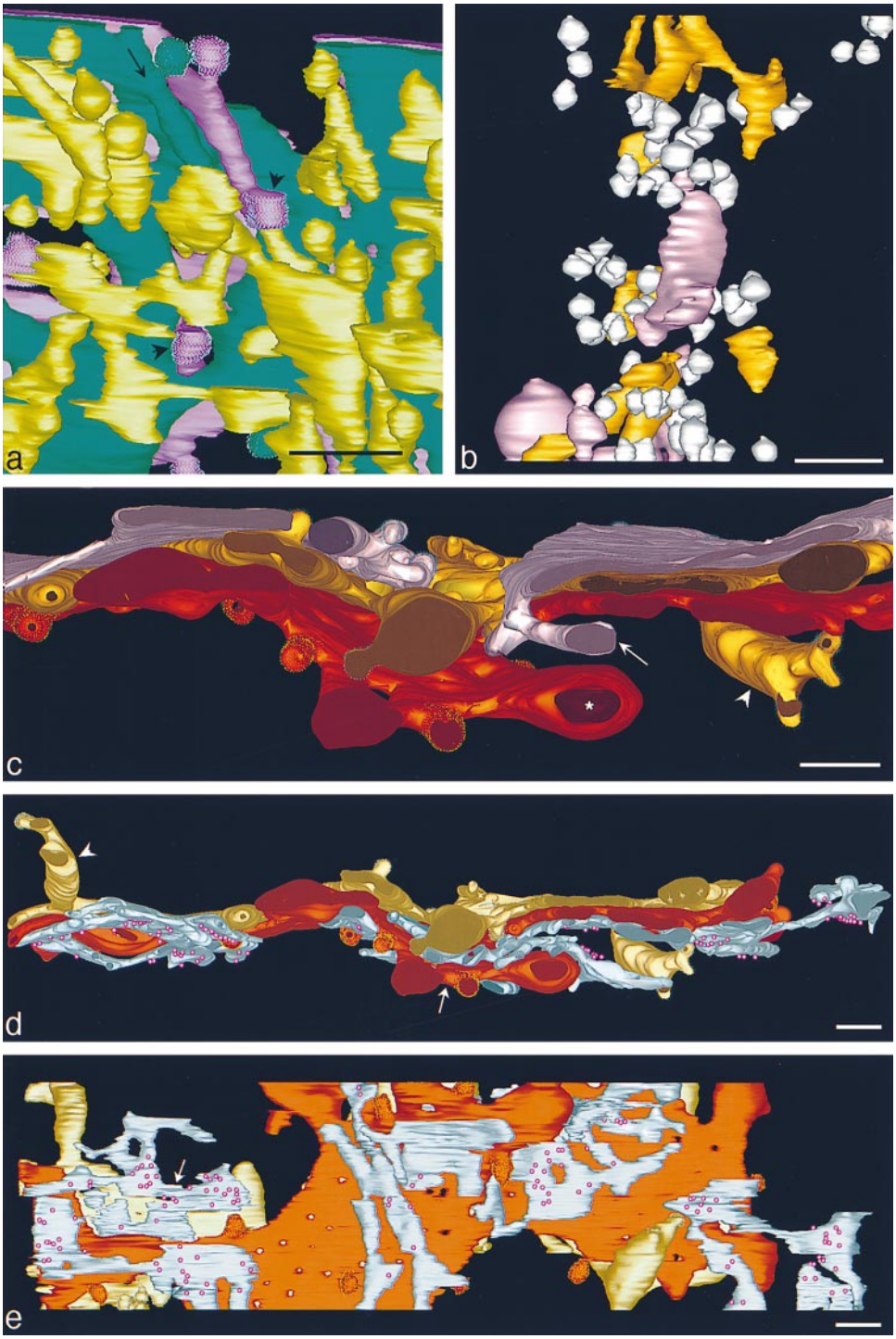

Figure 5. Relationships among different Golgi layers. (a) A higher magnification view of the cis side of the stack, showing parts of the ERGIC, the C1, and C2 cisternae oriented to display two tubules that extend from C2 past C1 and project into the ERGIC region. Both tubes end in non–clathrin-coated buds (short arrows). A tubule also projects from C1 and runs roughly parallel to the longer C2 tubule (long arrow). (b) Higher magnification view of the NCR. Many free non–clathrin-coated and uncoated vesicles (60–80 nm) and polymorphic elements fill this region. Some polymorphic elements resemble those of the ERGIC (gold), whereas the longer, rounded elements are different (pink). (c) A higher magnification view of the region where C5 projects a tubule past C6 and C7 into the space trans to the Golgi stacks (arrow). A tubule from C6 is also evident (arrowhead) and a lobule is protruding from C7 (star). (d and e) Two views of the trans Golgi showing the position of the trans ER relative to C6 and C7. The trans ER has ribosomes on only its free side (see also Fig. 3, bottom), and it is flattened against regions of both C6 (e, arrow) and C7 in a manner similar to the association between adjacent Golgi cisternae. The trans ER also wraps around C7 (d, arrow). The C7 cisterna covers most of the NCR. (e) Two tubules extend from C6: one projects in the trans direction, over C7 and the trans ER, where it branches and produces three non–clathrin-coated buds. The other projects in the cis direction, past all five previous cisternae, into the ERGIC region, where it ends in a non–clathrin-coated bud (see also Fig. 1 c). Bars, 250 nm.

Quantitative Analyses of Structural Parameters Can Be Used to Distinguish Cisternae

The gallery of images in Fig. 3 demonstrates the extent of structural variability among the modeled Golgi cisternae. We have quantified several structural parameters of the individual cisternae, some of which can be used to distinguish them. The surface areas of the reconstructed cisternae are remarkably similar, varying by <15% (Fig. 7 a). In contrast, the volumes of the cisternae differ by as much as 50% (Fig. 7 b), with C1 and C7 having the greatest volumes, C2 and C6 being ~20% less, and C3–5 having the smallest volumes. The ERGIC elements collectively have a markedly smaller surface area and volume than any of the Golgi cisternae.

The cisternae differ significantly in the size, density, and distributions of the openings that penetrate them (Figs. 7 c and 8). The distribution of opening sizes for all cisternae (Fig. 8 a) shows three modes, so the openings can be subdivided into "fenestrae" (<65 nm), "small holes" (65–100 nm), and "large holes" (>100 nm), that form the wells. The distribution of fenestral sizes changes progressively

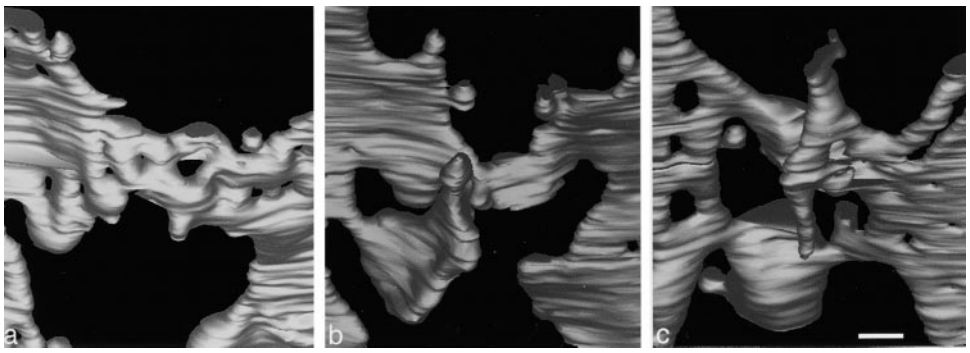

Figure 6. Components of the NCR attached to cisternae, including bridges, buds, and projecting tubules. a–c show views of the relevant parts of C1, C3, and C6, respectively. The complexity of these structures suggests that they are highly dynamic. Bar, 100 nm.

from cis to trans (see Figs. 7 and 8 for details). Thus, in cryofixed specimens, cisternal openings constitute a quantifiable trait that differs between cisternae.

The types and numbers of coated buds are additional quantifiable parameters that distinguish Golgi cisternae. As seen most clearly in Fig. 3, the coated buds on C7 are all clathrin coated (yellow stippling), whereas those on all other cisternae are exclusively of the nonclathrin type (blue stippling). None of the cisternae exhibits a mixture of clathrin- and non–clathrin-coated buds. The summed volumes of all the buds on a given cisterna are uniformly lower for the C1–C6 cisternae than for C7 (data not shown). (Fig. 7 d) The numbers of buds per cisterna vary in the cis-to-trans direction, with the highest numbers associated with C1 and C2, a gradual decrease from C3 to C5, and a leveling off in C6 and C7.

The two trans-most cisternae also differ from the preceding cisternae in less quantifiable ways (Figs. 3 and 5). Whereas the C1–C5 cisternae are all fairly flat and display a typical cisternal architecture that is interrupted only by well-forming holes, C6 is structurally variegated. It has two unusually shaped bridges that connect its parts across the NCR (Fig. 6 c); it includes a higher proportion of the 65–100-nm class of holes, bulging margins, and both cis- and trans-pointing tubular extensions (Fig. 5 d). The C7 cisterna presents a broad, undulating central region that covers part of the noncompact region. Some of its marginal domains appear inflated. Finally, as mentioned before, only C6 and C7 form close contacts with trans ER.

Based on these morphological features, the seven cisternae can be subdivided into two cis (C1 and C2), two medial (C3 ands C4), and two trans (C6 and C7) cisternae, accompanied by one cisterna (C5) that possesses both medial and translike properties. The evidence supporting these assignments rests, in addition to cisternal position, on the quantitative analyses presented above, the presence of tubules emanating from certain cisternae into the ERGIC and TGN regions, and the appositional interactions with trans-ER membranes.

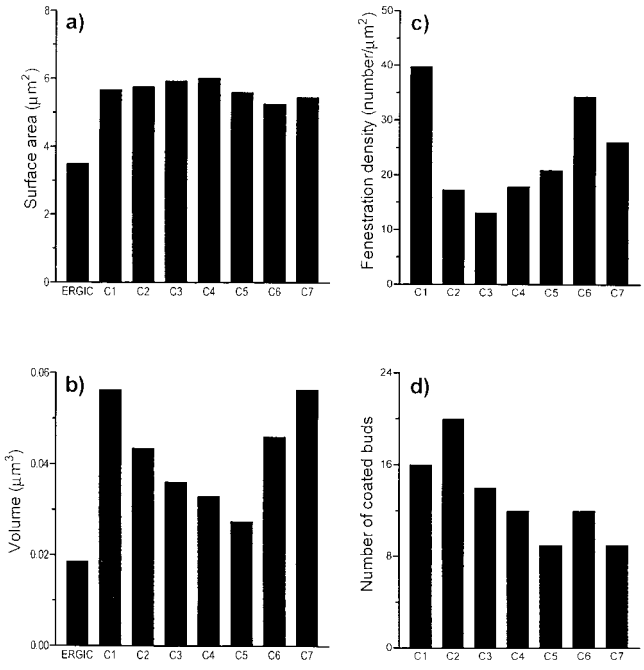

Figure 7. Comparative data on (a) surface area, (b) volume, (c) density of fenestrae, and (d) number of coated buds for the ERGIC and C1–C7 cisternae.

Discussion

Ever since Camillo Golgi first described the "Apparato reticolare interna" (Golgi, 1898), this organelle has been studied intensively (reviewed by Berger, 1997). Bursts of new information have often followed improvements in technology. Our use of two advanced structural methods (rapid freezing and dual-axis HVEM tomography) has likewise provided new information about Golgi architecture and novel insights into the relationships between its structure and its function. Many of our findings are summarized in Fig. 9. Highlights of the data include: detailed qualitative and quantitative information about the architecture of the different types of Golgi cisternae, including their buds, fenestrae, surface areas, and volumes; the description of tubules projecting from multiple cis and trans cisternae; the identification of polymorphic elements in the NCR; a characterization of the membranous elements of the ERGIC; the demonstration and 3-D description of specialized ER that is closely associated with the trans cisternae; and a quantitative analysis of the vesicles seen close to the Golgi stacks.

Our Model Confirms and Extends Published Ideas about Golgi Organization

As in most published work, cisternae form the basic units

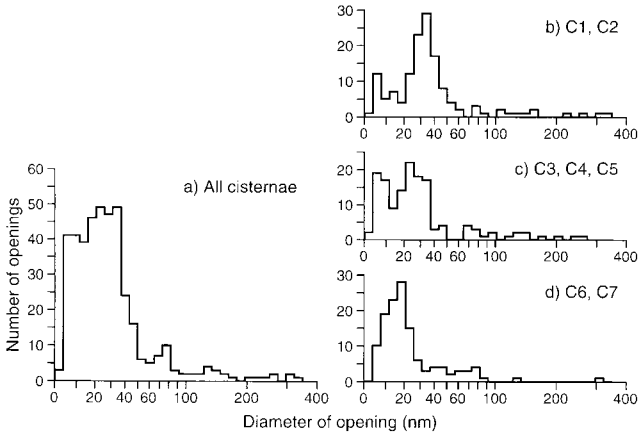

Figure 8. Histograms describing the average diameters of openings in Golgi cisternae: (a) all cisternae in the model, (b) the cis cisternae (C1 and C2), (c) the medial cisternae (C3–C5), and (d) the trans-most cisternae (C6 and C7). The area of each opening was measured and used to determine the diameter of an equivalent circle. Most of the fenestrae in C1 and C2 (b) have diameters between 25 and 50 nm (mode 34 nm), while those in C6 and C7 (d) range from 10 to 30 nm (mode 18 nm). The distributions for C1–C5 (b and c) show a distinct population of very small fenestrae (~8 nm), which are either absent or merged with the main peak in C6 and C7.

of this Golgi reconstruction. The region modeled contains two compact regions, each composed of seven cisternae that lie on either side of an NCR. Tubular bridges connect the two parts of cisternae C1, C3, and C6, but there are no connections between nonequivalent cisternae. Only the trans-most cisterna, C7, retains its sheet-like architecture over most of the NCR (Fig. 2). Photobleaching experiments have shown that Golgi membrane proteins tagged with the green fluorescent protein can diffuse along the entire Golgi ribbon within equivalent cisternae (Cole et al., 1996), which suggests that even the cisternae without apparent bridges are connected, perhaps outside the volume reconstructed. Alternatively, bridges may be transient, as suggested by the closeness of the ends of the "fragmented" bridge in C2.

Fenestrae (openings with diameters <65 nm) are common to all cisternae. The distributions of their sizes in different cisternae (Fig. 8) suggest that fenestra geometry is regulated. The functions of fenestrae remain unknown, but we identify three possibilities: they may serve as "spot welds" to control cisternal swelling, they may aid in the formation of buds by increasing the curvature of cisternal margins, and/or they may provide efficient pathways for diffusion from the membrane on one side of a cisterna to the other. We confirm the existence of cis-Golgi wells (Rambourg and Clermont, 1997), and we also identify smaller channels that open to the lateral and trans sides of a compact region. The prevalence of buds and vesicles in cis wells suggests that they are pathways for membrane traffic, possibly in both the anterograde and retrograde directions, though closure on the trans side eliminates the possibility of trans-Golgi exit by this route.

The medial cisternae in this reconstruction (C3, C4, and perhaps C5) lack some of the more striking structural elements of the cis and trans cisternae. They are less fenestrated, and their fenestrae are of intermediate size (Figs. 7 and 8). When viewed together, these cisternae exhibit cis-to-trans gradients in all of the quantified parameters in Fig. 7, except for surface area. Excepting C5, they lack the striking tubular extensions that are found on cis and trans cisternae.

The noncompact region in our model is more complex than previous data have suggested. In addition to the bridging tubules that connect equivalent cisternae from adjacent compact regions, it contains vesicles and polymorphic elements, some of which resemble components of the ERGIC. The extent to which its polymorphic elements contribute to membrane trafficking is, however, unknown. The trans side of the NCR is partially occluded by C7, which may bias its vesicle trafficking toward the cis side. Indeed, it and the cis-Golgi wells may be quantitatively different manifestations of similar Golgi specializations. The structural complexity of the NCR suggests, however, that this region plays additional, yet-to-be characterized roles in Golgi function.

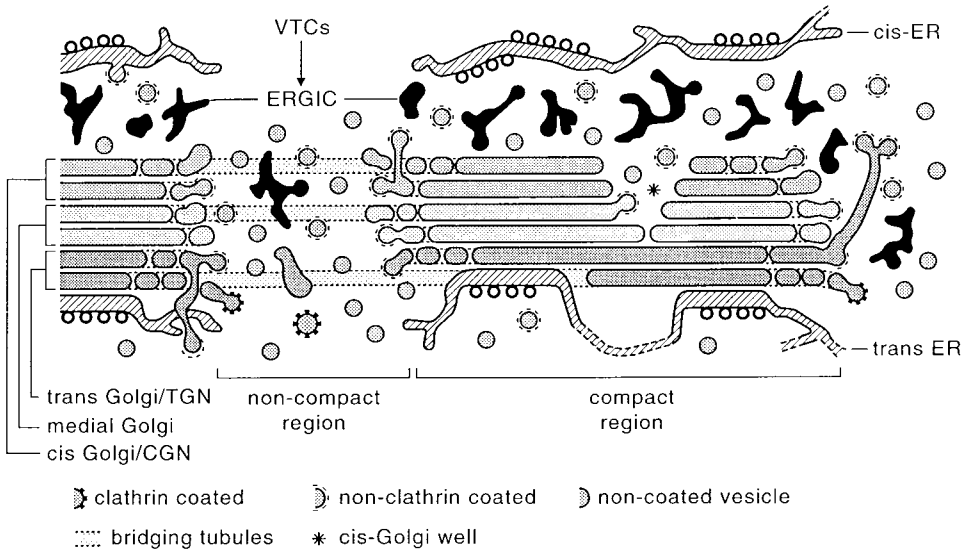

Figure 9. Interpretative model of the structural organization of the mammalian Golgi apparatus based on the data presented in this paper.

All of the Golgi cisternae display budding vesicle profiles. All but 2 of the 92 buds in our model arise from the edges of cisternae, emerging from either their margins or from the rims of their wells. The highest numbers of buds are on the cis cisternae, followed by a decline towards the trans cisternae (Fig. 7 d); this pattern is consistent with the idea that buds are primarily involved in retrograde transport (Lowe and Kreis, 1998). However, the presence of large numbers of non–clathrin-coated and noncoated free vesicles surrounding the trans side of the stacks (Fig. 3, bottom) suggests that some of the buds are destined for exit from the Golgi. Future refinements in staining methods should permit further subclassification of coats beyond the nonclathrin and clathrin coats distinguished here.

The ERGIC Can Be Organized as an Element of the Golgi Complex

The layer of our model called ERGIC consists of 44 branched, polymorphic membranous elements situated between the cis ER and the cis-most Golgi cisterna (Figs. 1, c and d, 3, and 5 a). ERGIC was first identified in experiments that used low temperature (15°C) to stall the transport of newly synthesized Semliki Forest virus spike glycoproteins (Saraste and Kuismanen, 1984). Markers for this compartment have been identified in two species: p58 in rat and p53 in human cells (Saraste et al., 1987; Schweitzer et al., 1988). Further work has identified "vesicular tubular clusters" (VTCs), which are defined as "export complexes" that form around ER "exit sites" dispersed throughout the cytoplasm (Bannykh et al., 1996). At these sites, newly synthesized secretory and membrane proteins are sorted and packaged into COPII-coated vesicles that subsequently fuse into larger structures from which ER components are recycled via COPI-coated vesicles. The p58/p53 antigen that identifies ERGIC is also a marker for VTCs, so ERGIC and VTCs are considered to be related structures. VTCs have been shown to travel along microtubules and flatten onto the cis face of the Golgi (Presley et al., 1997; Scales et al., 1997).

In our reconstruction, the polymorphic structures of the ERGIC layer resemble elements from VTCs. They also lie adjacent to the cis-most cisterna, though most are not flattened. We suggest that the ERGIC layer of our model is composed of parts of VTCs that have arrived at the Golgi but were frozen before they had flattened on the Golgi stack. The clustering of ERGIC over compact regions of the underlying cisterna suggests an interaction with the cis-most Golgi cisterna and may reflect an intermediate stage in the formation of a new cisterna (Fig. 1, c and d).

Cis and Trans Cisternae Possess Tubular Extensions, but Do Not Display a Network Architecture

Extensive evidence suggests that the cis and trans faces of compact Golgi regions are dynamic and structurally complex. With stereo EM of hyperosmicated specimens, the cis-most cisterna appears as a reticular network with occasional tubular structures extended from it (Lindsey and Ellisman, 1985; reviewed by Rambourg and Clermont, 1997). Tubules have also been observed in vivo projecting from the cis side after antibody injection (Kreis, 1990), and from the trans side, using fluorescent lipids (Cooper et al., 1990) or chimeras containing the green fluorescent protein (Cole et al., 1996; Sciaky et al., 1997; Scales et al., 1997; Presley et al., 1998). These tubules are dynamic, extending and breaking off from the rest of the Golgi. Our images of the cis-Golgi region include tubules (Fig. 5 a), although the ones we have seen are smaller than those visualized by light microscopy. We have not, however, seen the reticulum that is observed in hyperosmicated specimens. This discrepancy might be due to our not having examined enough specimens, but other Golgi regions, visualized in fast-frozen, freeze-substituted cells by HVEM tomography, also lack this feature (data not shown). Experimental conditions that extract or destroy Golgi membrane proteins (e.g., hyperosmication) may destabilize cisternal architecture, enlarging fenestrae, promoting the formation of tubules, and converting fenestrated cisternae into planar tubular networks (Cunningham et al., 1974). We therefore think it likely that reticulation of the cis-Golgi region is induced by preparative procedures.

This interpretation suggests a rethinking of the concept of a "cis-Golgi Network" (CGN; Duden et al., 1991; Mellman and Simons, 1992). Our data are consistent with the idea that the two cis-most cisternae, together with their associated tubules, carry out the functions attributed to the CGN, but that there is no cis-Golgi network per se.

The trans sides of compact Golgi regions have also been shown to display projecting tubules. The concept of a "trans-Golgi network" was introduced by Griffiths et al. (1995) to discuss a compartment where the three major classes of proteins that move through the Golgi might be sorted and packaged for export; proteins destined for the plasma membrane (via constitutive vesicles) would be separated from proteins to be secreted (via regulated granules) and those destined for lysosomes (through clathrin-coated vesicles). This compartment was described as a tubular reticulum on the trans side of a Golgi stack. Contrary to this description, we do not see a reticulum of interconnected trans tubules, neither in this model nor in our earlier study of the TGN (Ladinsky et al., 1994), nor in other reconstructions of fast-frozen, freeze-substituted material (data not shown).

As with the CGN, we suspect that preparative methods may contribute to the extent to which Golgi cisternae appear reticulated. The TGN has usually been visualized with a specific structural marker: enzyme cytochemistry to reveal a phosphatase, photoconversion of a fluorescent lipid to visualize the trans Golgi more generally, or immunolocalization with a Golgi-specific antibody. All such work has been based on aldehyde-fixed material, so the possibility of membrane rearrangements during specimen preparation cannot be excluded. Moreover, cytochemical staining often involves diaminobenzidine, which is sufficiently hydrophobic to partition into lipid bilayers, expanding them artificially (Boos and Staehelin, 1981). Taken together, these results suggest that, whereas cytochemical staining may provide highly relevant data in terms of enzyme localization, such procedures are less than ideal for defining cisternal architecture.

Our model is also at variance with the classical description of TGN in its paucity of tubules that project from trans-Golgi cisternae. This difference may be a result of

our small sample size and represent only the specific regions that have so far been reconstructed. Other regions of the Golgi ribbon, in this or in other cells, may well show more tubules. Further work will be required to assess this possibility.

Our Model Contains at Least Two Types of Trans Cisternae

Cisternae C6 and C7 are structurally different, both from each other and from the other cisternae of our model (Fig. 3). The diameter and density of their fenestrae are distinct (Figs. 7 c and 8 d), their volumes are larger that those of C3–C5 (Fig. 7 b), and their intimate association with trans ER is unique (Fig. 5, d and e). They and C5 (Fig. 5 c) project tubules into the regions trans from the Golgi stacks. The most significant difference between these cisternae is that C7 buds exclusively clathrin-coated vesicles, while C5 and C6 bud only vesicles with nonclathrin coats. C7 is also unique in covering much of the trans side of the NCR. C6 is the most structurally variegated of all the cisternae in this model. It includes two unusually shaped bridges across the NCR, and it gives rise to two extensive tubules: one that curves around C7 and the trans ER to end with three budding profiles (Fig. 5 c, arrowhead), and another that extends past all five of the preceding cisternae to end with a budding profile near the ERGIC (Fig. 5 d, arrowhead). For all these reasons, we consider C6 and C7 to be distinct trans cisternae. The trans-reaching tubule on C5 (Fig. 5 c, arrow) adds a translike property to this medial cisterna, thereby giving it a transitional character.

The idea of distinguishable trans cisternae is not new. A cornerstone of the GERL hypothesis of Novikoff et al. (1971) was that cytochemistry identified different enzymes in the two trans-most cisternae (see also Hand and Oliver, 1977). When the dominant localization technology changed to immunogold labeling of frozen thin sections, however, differences in the trans cisternae were no longer observed (e.g., Geuze et al., 1987; Griffiths et al., 1995). This may be due in part to the resolution of the technique: Golgi cisternae are separated by ~20 nm, and the labeling method used has a resolution of about that magnitude (Griffiths et al., 1995). Therefore, even if a molecule is localized to a single cisterna, its appearance might "spill over" to the next cisterna.

Functional Implications of Having Two Types of Trans Cisternae: They and Their Tubules May Carry Out the Functions of the TGN

Clathrin is involved exclusively in packaging products destined for the endosomal/lysosomal pathway (reviewed by Traub and Kornfeld, 1997). The finding that C7 both uniquely and exclusively produces clathrin-coated buds (Figs. 3 and 5) indicates that this cisterna packages molecules for the lysosomal pathway. The presence of long tubules and extensive nonclathrin buds on the penultimate trans cisterna (C6) suggests that it is the most probable site for packaging molecules that are destined to the plasma membrane.

Ladinsky et al. (1994) showed that individual tubules that are continuous with different trans cisternae produced buds that were either clathrin coated or covered with a lace-like coat, but never a mixture of the two. These observations suggested that sorting of molecules must occur before the formation of such TGN tubules, but they raised the question of whether a single cisterna might produce vesicles with only one or two coat types. Our new data indicate that each cisterna produces vesicles of only one coat type. This allows us to extend our hypothesis about the mechanism for exit from the Golgi to suggest that molecules destined for the plasma membrane are sorted to a different cisterna than those targeted for the endosomal/lysosomal pathway; from each of these cisternae they are then packaged for transport. In this model, two or more trans cisternae are involved in exit from the Golgi, so together they correspond to the TGN. As discussed above for the CGN, there does not appear to be a TGN compartment that is distinct from the trans cisternae and their tubules.

This hypothesis about the mechanism of Golgi exit would be strengthened if we were able to distinguish the lacelike coat from other coat types, which we cannot. Three factors may have contributed to this problem. First, rapid freezing and freeze substitution, which preserves the complexity of cytoplasm with little if any extraction, may have obscured the lacelike coat. Coat structures are best seen in samples where cytoplasm has been extracted (Futter et al., 1998). Second, tannic acid was present in the freeze-substitution medium to enhance the contrast of membranes and coats. The deposition of tannic acid may have masked the fine detail of the lacelike coat, making it indistinguishable from COP coats. Third, the BODIPY (4,4-difluoro-4-bora-3a,4a-diaza-s-indacene)-ceramide used as a stain in the previous study (Ladinsky et al., 1994) may have enhanced, or even created, the appearance of the lacelike coat. Each of these factors is now being examined.

It is important to note that there are other possible explanations for why the trans-most cisterna of our model exhibits only clathrin-coated buds. Temporal differences in cisternal activities could result in a cisterna's cycling between phases of sorting and packaging of molecules destined for different pathways. We think this explanation is unlikely because multiple trans cisternae form tubules, suggesting that multiple trans cisternae can function like the TGN in export from the Golgi (Ladinsky et al., 1994; Rambourg and Clermont, 1997).

The Close Association of Trans-ER with Trans-Golgi Cisternae May Provide Sites for Lipid Transfer

A close apposition of trans ER with the two trans-most Golgi cisternae is a prominent feature of fast-frozen/freeze-substituted NRK cells and is commonly seen in thin sections of PtK and CHO cells preserved in a similar manner (data not shown). The apposition has also been described in numerous chemically fixed cells (Novikoff et al., 1971; Hand and Oliver, 1977; Thorne-Tjomsland et al., 1991; Rambourg and Clermont, 1997). Its roles in Golgi function should therefore be explored.

We propose that this close apposition allows an exchange of lipids either to or from the trans-Golgi membranes by a nonvesicular, intermembrane, lipid-hopping mechanism. Precedent for such a hypothesis is found in

the transfer of phosphatidylserine from ER to mitochondria for the production of phosphatidylethanolamine, a major component of mitochondrial membranes (Vance and Shiao, 1996). Such a mechanism may also account for the movement of diacylglycerol from the trans Golgi to the ER, where it serves as a precursor for the generation of new phosphotidylcholine (Pagano, 1990). A nonvesicular type of lipid recycling from the plasma membrane to the ER has been postulated to occur in plants, based both on fluorescent lipid redistribution studies and on the visualization of transient appositions between these two membrane systems in cryofixed cells (Staehelin, 1997). These factors, together with the obvious need for lipids to package exported proteins, encourage us to consider mechanisms for lipid transfer directly between the ER and the trans Golgi.

Evidence for a lipid-hopping mechanism is found in the transfer rates of newly synthesized phospholipids from ER to the plasma membrane (Kaplan and Simoni, 1985a,b): $t_{1/2}$ = 2 min for phospholipids at 25°C, while newly synthesized cholesterol takes ~10 min. The transit of phospholipids is thus too fast to occur via conventional membrane traffic from ER to Golgi to the plasma membrane, but it could be accomplished by the insertion of lipids directly at the TGN. Such transfer could be mediated by polypeptides like the antibacterial polymyxin B, which at very low mole fractions (~0.0005, or only a few molecules per vesicle) can form stable contacts between vesicles containing anionic phospholipids and stimulate lipid exchanges through these contacts at ~300 molecules/s (Cajal et al., 1996). We conclude that lipid transfer is a plausible reason for the close apposition between ER and trans-Golgi cisternae.

Implications of Our Model for Golgi Trafficking Hypotheses

The novel data presented here place structural constraints on the models now being considered for transit to, through, and from the Golgi complex. The hypothesis of tubular transport suggests that anterograde transport between successive cisternae is mediated by transient tubular connections (Weidman et al., 1993). Since we found no connections between nonequivalent cisternae, nor any bridging tubules with branches to two or more cisternae, our data do not support this theory.

Transport based on tubules with associated buds almost certainly occurs in the Golgi, but it seems to function in transport out of the Golgi in both the cis and trans directions. The fact that both cis- and trans-projecting tubules can pass one or more cisternae suggests that Golgi traffic need not visit all compartments on its way through or out of the Golgi. We surmise that more extensive tubules might also project from the trans-most Golgi cisterna at some time other than that of our freezing. All these tubules are likely to correspond to the ones seen in vivo, which have contributed to the concepts of CGN and TGN.

It is more difficult to provide insight into the processes of vesicular transport, as vesicles are abundant in our model as well as in many published images. All cisternae have buds, indicating the formation of vesicles, so our data are consistent with vesicular traffic for both directions of intra-Golgi transport. There is also a wealth of vesicles at both the cis and trans faces of Golgi stacks, suggesting that both vesicles and tubules are involved in exit from the Golgi.

The cisternal progression/maturation model posits that new cis/CGN cisternae are constantly being formed from VTCs (ERGIC), so indications of new cisternae should be seen on a frequent basis (Sesso et al., 1994; Bonfanti et al., 1998). The polymorphic ERGIC elements in this reconstruction are poorly organized and show no sign of fusion with the C1 cisterna or with each other to form a new cisterna. These elements may, however, represent VTCs just after their arrival at the cis-most cisterna. Delivery of additional VTCs, followed by their fusion and flattening beyond that seen in the ERGIC elements of our model, could eventually form a new cisterna. The remarkable patterning of ERGIC over the cis-most cisterna suggests this possibility and encourages further consideration of this model.

Final characterization of the pathways for Golgi traffic will require work that combines reliability of specimen preparation and 3-D visualization, which characterize the current study, together with the identification of the specific molecular components that play key transport roles. Thus, our study forms a framework for future structural and experimental work that will focus on the locations and rearrangements of particular Golgi molecules.

We thank Jim Kremer for taking tilt series micrographs and for software development improvements.

This work was supported by grant RR00592 to J.R. McIntosh from the National Center for Research Resources of the National Institutes of Health (NIH), and by NIH grants GM18639 to L.A. Staehelin and GM42629 to K.E. Howell.

Received for publication 3 December 1998 and in revised form 1 February 1999.

References

Bannykh, S.I., and W.E. Balch. 1997. Membrane dynamics at the endoplasmic reticulum-Golgi interface. *J. Cell Biol.* 138:1–4.

Bannykh, S.I., T. Rowe, and W.E. Balch. 1996. The organization of endoplasmic reticulum export complexes. *J. Cell Biol.* 135:19–35.

Becker, B., B. Böllinger, and M. Melkonian. 1995. Anterograde transport of algal scales through the Golgi complex is not mediated by vesicles. *Trend Cell Biol.* 5:305–307.

Bonfanti, L., A.A. Mironov, Jr., J.A. Martínez-Menárguez, O. Martella, A. Fusella, M. Baldessarre, R. Buccione, H.J. Geuze, A.A. Mironov, and A. Luini. 1998. Procollogen traverses the Golgi stack without leaving the lumen of cisternae: evidence for cisternal maturation. *Cell.* 95:993–1003.

Berger, E.G. 1997. The Golgi apparatus: from discovery to contemporary studies. *In* The Golgi Apparatus. E.G. Berger and J. Roth, editors. Birkhäuser Verlag, Basel, Switzerland. 1–35.

Boos, W., and L.A. Staehelin. 1981. Ultrastructural localization of the maltose-binding protein within the cell envelope of *Escherichia coli*. *Arch. Mikrobiol.* 129:240–246.

Cajal, Y., J. Rogers, O.G. Berg, and M.K. Jain. 1996. Intermembrane molecular contacts by polymyxin B mediate exchange of phospholipids. *Biochemistry.* 35:299.

Clermont, Y., L. Xia, A. Rambourg, J.D. Turner, and L. Hermo. 1993. Transport of Casein submicelles and formation of secretion granules in the Golgi apparatus of epithelial cells of the lactating mammary gland of the rat. *Anat. Rec.* 237:235–363.

Cluett, E.B., S.A. Wood, M. Banta, and W.J. Brown. 1993. Tubulation of Golgi membranes in vivo and in vitro in the absence of BFA. *J. Cell Biol.* 120:15–24.

Cole, N.B., C.L. Smith, N. Sciaky, M. Terasaki, M. Edidin, and J. Lippincott-Schwartz. 1996. Diffusional mobility of Golgi proteins in membranes of living cells. *Science.* 273:797–801.

Cooper, M.S., A.H. Cornell-Bell, A. Chernjavsky, J.W. Dani, and S.J. Smith. 1990. Tubulovesicular processes emerge from *trans*-Golgi cisternae, extend along microtubules and interlink adjacent *trans* Golgi elements into a reticulum. *Cell.* 61:135–145.

Cunningham, W., L.A. Staehelin, R.W. Rubin, R. Wilkins, and M. Bonneville. 1974. Effects of phosphotungstate negative staining on the morphology of isolated Golgi apparatus. *J. Cell Biol.* 62:491–504.

Dahan, S., J.P. Ahluwalia, L. Wong, B.E. Posner, and J.J.M. Bergeron. 1994. Concentration of intracellular hepatic apolipoprotein E in Golgi apparatus saccular distensions and endosomes. *J. Cell Biol.* 127:1859–1869.

Duden, R., G. Griffiths, R. Frank, P. Argos, and T.E. Kreis. 1991. Beta-COP, a 110 kd protein associated with non–clathrin-coated vesicles and the Golgi complex, shows homology to beta-adaptin. *Cell*. 649:649–665.

Farquhar, M.G., and H.-P. Hauri. 1997. Protein sorting and vesicular traffic in the Golgi apparatus. *In* The Golgi Apparatus. E.G. Berger and J. Roth, editors. Birkhäuser Verlag, Basel, Switzerland. 63–129.

Farquhar, M.G., and G.E. Palade. 1981. The Golgi apparatus (complex)–(1954-1981)–from artifact to center stage. *J. Cell Biol.* 91:77s–103s.

Futter, C.E., A. Gibson, E.H. Allchin, S. Maxwell, L.J. Ruddock, G. Odorizzi, D. Somingo, I.S. Trowbridge, and C.E. Hopkins. 1998. In polarized MDCK cells basolateral vesicles arise from clathrin-γ-adaptin–coated domain on endosomal tubules. *J. Cell Biol.* 141:611–623.

Geuze, H.J., J.W. Slot, and A.L. Schwartz. 1987. Membranes of sorting organelles display lateral heterogeneity in receptor distribution. *J. Cell Biol.* 104:1715–1723.

Gilkey, J.C., and L.A. Staehelin. 1986. Advances in ultrarapid freezing for the preservation of cellular ultrastructure. *J. Electron Microsc. Tech.* 3:177–210.

Glick, B.S., and V. Malhotra. 1998. The curious status of the Golgi apparatus. *Cell*. 95:883–889.

Golgi, C. 1898. Sur la structure des cellules nerveuses des ganglions spinaux. *Archives Italiennes de Biologie*. 30:60–71.

Griffiths, G., and K. Simons. 1986. The trans-Golgi network: sorting at the exit site of the Golgi complex. *Science.* 234:438–443.

Griffiths, G., S.D. Fuller, R. Back, M. Hollinshead, S. Pfeiffer, and K. Simons. 1989. The dynamic nature of the Golgi complex. *J. Cell Biol.* 108:277–297.

Griffiths, G., R. Pepperkok, L. Krijnse, and T.E. Kreis. 1995. Immunocytochemical localization of b-COP to the ER-Golgi boundary and the TGN. *J. Cell Sci.* 108:2839–2856.

Hand, A.R., and C. Oliver. 1977. Relationship between the Golgi apparatus, GERL, and secretory granules in acinar cells of the rat exorbital lacrimal gland. *J. Cell Biol.* 74:399–413.

Kaplan, M.R., and R.D. Simoni. 1985a. Intracellular transport of phosphatidylcholine to the plasma membrane. *J. Cell Biol.* 101:441–445.

Kaplan, M.R., and R.D. Simoni. 1985b. Transport of cholesterol from the endoplasmic reticulum to the plasma membrane. *J. Cell Biol.* 101:446–453.

Kreis, T.E. 1990. Role of microtubules in the organisation of the Golgi apparatus. *Cell Motil. Cytoskelet.* 15:67–70.

Kremer, J.R., D.N. Mastronarde, and J.R. McIntosh. 1996. Computer visualization of three-dimensional image data using IMOD. *J. Struct. Biol.* 116:71–76.

Ladinsky, M.S., J.R. Kremer, P.S. Furcinitti, J.R. McIntosh, and K.E. Howell. 1994. HVEM tomography of the trans-Golgi network: structural insights and identification of a lace-like vesicle coat. *J. Cell Biol.* 127:29–38.

Lindsey, J.D., and M.H. Ellisman. 1985. The neuronal endomembrane system II. The multiple forms of the Golgi apparatus *cis* element. *J. Neurosci.* 5:3124–3134.

Lowe, M., and T.E. Kreis. 1998. Regulation of membrane traffic in animal cells by COPI. *Biochim. Biophys. Acta.* 1404:53–66.

Luther, P.K., M.C. Lawrence, and R.A. Crother. 1988. A method for monitoring the collapse of plastic sections as a function of electron dose. *Ultramicroscopy*. 24:7–18.

Mastronarde, D.N. 1997. Dual-axis tomography: an approach with alignment methods that preserve resolution. *J. Struct. Biol.* 120:343–352.

Mellman, I., and K. Simons. 1992. The Golgi complex: *in vitro* veritas? *Cell.* 68: 829–840.

Mironov, A.A., P. Weidman, and A. Luini. 1997. Variations on the intracellular transport theme: maturing cisternae and trafficking tubules. *J. Cell Biol.* 138: 481–484.

Mironov, A., Jr., A. Luini, and A. Mironov. 1998. A synthetic model of intra-Golgi traffic. *FASEB J.* 12:249–252.

Morré, D.J., and T.W. Keenan. 1997. Membrane flow revisited: what pathways are followed by membrane molecules moving through the Golgi apparatus? *Bioscience.* 47:489–498.

Novikoff, P.M., A.B. Novikoff, N. Quintana, and J.-J. Hauw. 1971. Golgi apparatus, GERL, and lysosomes of neurons in rat dorsal root ganglia, studies by thick section and thin section cytochemistry. *J. Cell Biol.* 50:859–886.

Orci, L., V. Malhotra, M. Amherdt, T. Serafini, and J.E. Rothman. 1989. Dissection of a single round of vesicular transport: sequential intermediates for intercisternal movement in the Golgi stack. *Cell.* 56:357–368.

Orci, L., M. Stamnes, M. Ravazzola, M. Amherdt, A. Perrelet, T.H. Sollner, and J.E. Rothman. 1997. Bidirectional transport by distinct populations of COPI-coated vesicles. *Cell*. 90:335–349.

Pagano, R.E. 1990. Lipid traffic in eukaryotic cells: mechanisms for intracellular transport and organelle-specific enrichment of lipids. *Curr. Opin. Cell Biol.* 2:652–663.

Palade, G.E. 1975. Intracellular aspects of the process of protein secretion. *Science.* 189:347–358.

Penczek, P., M. Marko, K. Buttle, and J. Frank. 1995. Double-tilt electron tomography. *Ultramicroscopy*. 60:393–410.

Presley, J.F., N.B. Cole, T.A. Schroer, K. Hirschberg, K.J.M. Zaal, and J. Lippincott-Schwartz. 1997. ER-to-Golgi transport visualization in living cells. *Nature.* 389:81–85.

Presley, J.F., C. Smith, K. Hirshberg, C. Miller, N.B. Cole, K.J.M. Zaal, and J. Lippincott-Schwartz. 1998. Golgi membrane dynamics. *Mol. Biol. Cell.* 9:1617–1626.

Radermacher, M. 1992. Weighted back-projection methods. *In* Electron Tomography. J. Frank, editor. Plenum Publishing Corp., New York. 91–115.

Rambourg, A., and Y. Clermont. 1990. Three-dimensional electron microscopy: structure of the Golgi apparatus. *Eur. J. Cell Biol.* 51:189–200.

Rambourg, A., and Y. Clermont. 1997. Three-dimensional structure of the Golgi apparatus in mammalian cells. *In* The Golgi Apparatus. E.G. Berger and J. Roth, editors. Birkhäuser Verlag, Basel, Switzerland. 37–61.

Rambourg, A., Y. Clermont, and L. Hermo. 1979. Three-dimensional architecture of the Golgi apparatus in Sertoli cells of the rat. *Am. J. Anat.* 154:455–476.

Roth, J., D.J. Taatjes, J.M. Lucocq, J. Weinstein, and J.C. Paulson. 1985. Demonstration of an extensive *trans*-tubular network continuous with the Golgi apparatus stack that may function in glycosylation. *Cell.* 43:287–295.

Rothman, J.E. 1994. Mechanisms of intracellular transport. *Nature.* 372:55–63.

Saraste, J., and E. Kuismanen. 1984. Pre- and post-Golgi vacuoles operate in the transport of Semliki Forest virus membrane glycoproteins to the cell surface. *Cell.* 38:535–549.

Saraste, J., G.E. Palade, and M.G. Farquhar. 1987. Antibodies to rat pancreas Golgi subfractions: identification of a 58-kD *cis*-Golgi protein. *J. Cell Biol.* 105:2021–2030.

Scales, S.J., R. Pepperkok, and T.E. Kreis. 1997. Visualization of ER-to-Golgi transport in living cells reveals a sequential mode of action for COPII and COPI. *Cell.* 90:1137–1148.

Schekman, R., and L. Orci. 1996. Coat proteins and vesicle budding. *Science.* 271:1526–1539.

Schweitzer, A., J.A.M. Fransen, T. Bächi, L. Ginsel, and H.-P. Hauri. 1988. Identification, by a monoclonal antibody, of a 53-kD protein associated with a tubulo-vesicular compartment at the *cis*-side of the Golgi apparatus. *J. Cell Biol.* 264:1643–1653.

Sciaky, N., J. Presley, C. Smith, K.J.M. Zall, N.B. Cole, J.E. Moreiea, M. Terasaki, E. Siggia, and J. Lippincott-Schwartz. 1997. Golgi tubule traffic and the effects of Brefeldin A visualized in living cells. *J. Cell Biol.* 139:1137–1155.

Sesso, A., F.P. de Faria, E.S. Iwamura, and H. Correa. 1994. A three-dimensional reconstruction study of the rough ER–Golgi interface in serial thin sections of the pancreatic acinar cell of the rat. *J. Cell Sci.* 107:517–528.

Soto, G.E., S.J. Young, M.E. Martone, T.J. Deerinck, S. Lamont, B. Carragher, K.O. Hama, and M.H. Ellisman. 1994. Serial section electron tomography: a method for three-dimensional reconstruction of large structures. *Neuroimage.* 1:230–243.

Staehelin, L.A. 1997. The plant ER: a dynamic organelle composed of a large number of discrete functional domains. *Plant J.* 11:1151–1165.

Thorne-Tjomsland, G., Y. Clermont, and X.M. Tang. 1991. Glucose-6-phosphatase activity of endoplasmic reticulum and Golgi apparatus in spermatocytes and spermatids of the rat: an electron microscopic cytochemical study. *Biol. Cell.* 71:33–41.

Traub, L.M., and S. Kornfeld. 1997. The trans-Golgi network: a late secretory sorting station. *Curr. Opin. Cell Biol.* 9:527–533.

Vance, J.E., and Y.-J. Shiao. 1996. Intracellular trafficking of phospholipids: import of phosphatidylserine into mitochondria. *Anticancer Res.* 16:1333–1340.

Weidman, P., R. Roth, and J. Heuser. 1993. Golgi membrane dynamics imaged by freeze-etch electron microscopy: views of different membrane coatings involved in tubulation versus vesiculation. *Cell*. 75:123–133.